A New Boundary Closure Scheme for the Multiresolution Time-Domain (MRTD) Method

Pengfei Yao and Shan Zhao

***Abstract*—This paper introduces a novel boundary closure treatment for the wavelet based multiresolution time-domain (MRTD) solution of Maxwell's equations. Accommodating non-trivial boundary conditions, such as the Robin condition or time dependent condition, has been a challenging issue in the MRTD analysis of wave scattering, radiation, and propagation. A matched interface and boundary (MIB) method is introduced to overcome this difficulty. Several numerical benchmark tests are carried out to validate the MIB boundary scheme. The proposed boundary treatment can also be applied to other high order finite-difference time-domain (FDTD) approaches, such as the dispersion-relation-preserving (DRP) method. The MIB boundary scheme greatly enhances the feasibility for applying the MRTD methods to more complicated electromagnetic structures.**

***Index Terms*—Convergence of numerical methods, finite difference time domain methods.**

I. Introduction

It is well known that numerical dispersion is a major limiting factor for the applicability of the finite-difference time-domain (FDTD) scheme to electromagnetic problems involving electrically large structures. Typically, the dimensions of the scatterer in such problems greatly exceed the wavelength of the incident wave so that the grid size required by using the FDTD method could become prohibitively expensive. In order to circumvent this difficulty, numerical approaches that are able to accurately represent the wave solution by using only a few points per wavelength must be employed to relieve the computational cost. This motivates the development of many low dispersion or high order FDTD methods in the past two decades, including FDTD(2,4) scheme [1], wavelet based multiresolution time-domain (MRTD) methods [2], [3], Fourier pseudospectral time-domain (PSTD) methods [4], [5], dispersion-relation-preserving (DRP) FDTD methods [6], [7], and local spectral time-domain (LSTD) methods [8], [9], etc.

What are more related to the present paper are the MRTD methods, even though the proposed boundary closure scheme can be applied to other long stencil FDTD approaches, such as the DRP-FDTD or LSTD. The original MRTD schemes [2], [3] are derived using cubic spline Battle-Lemarie scaling and wavelet functions. When electromagnetic fields are expanded solely in terms of scaling functions, the corresponding MRTD scheme is usually called as an S-MRTD scheme, while W-MRTD scheme refers to a scheme in which both scaling and wavelet functions are used as basis functions. Since the orthogonal Battle-Lemarie wavelet family is not compactly supported, various MRTD methods using compactly supported wavelet expansions have been developed in the literature. For example, novel MRTD methods based on Coifman and Daubechies scaling functions have been introduced, respectively, in [10] and [11]. A general framework for constructing MRTD algorithms based on biorthogonal scaling and wavelet functions has been established in [12], with a particular realization given to the Cohen-Daubechies-Feauveau (CDF) biorthogonal wavelets. The stencil length of the Daubechies type MRTD methods can be adjusted by the number of vanishing moments, while the latter also determines the order of accuracy of the resulting MRTD spatial discretization [13]. In [14], a systematic procedure is proposed to update the time in the MRTD calculations by using a novel Runge-Kutta scheme so that an arbitrarily high order of convergence in both space and time could be realized. The Fourier dispersive error analysis of some MRTD schemes and a comparison with the standard high order FDTD schemes have been conducted in [15].

The MRTD methods all use wide stencils. Thus, special boundary treatments are required near boundaries where the MRTD approximation may refer to nodes outside the computational domain [16], [17]. Like other time-domain approaches, the perfectly matched layer (PML) absorbing boundary conditions can be naturally incorporated into the collocation procedure of the MRTD schemes [18], while the simple image principle is commonly used in the MRTD calculations to deal with perfect electric conducting (PEC) or perfect magnetic conducting (PMC) boundary conditions [2]. In order to handle the PEC conditions in different scenarios, several advanced boundary closure schemes [19]–[21] have been introduced to the MRTD analysis. The generalization of the image principle at the PEC walls of the multi-layer dielectric structures has been formulated in [19]. An elegant extension of the CDF-MRTD schemes to treat thin metallic irises or infinitely thin perfect electric walls has been presented in [20]. Modification of basis expansion has been suggested in [21] for the purpose of implementing the image principle for the MRTD methods with basis functions being non-symmetric and/or without interpolation property. In summary, the existing MRTD boundary treatments can only handle some regular boundary conditions, such as the PML, PEC, and PMC conditions. No general boundary

Manuscript received August 10, 2010; revised November 22, 2010; accepted February 15, 2011. Date of publication July 12, 2011; date of current version September 02, 2011. This work was supported in part by NSF grants DMS-0616704, DMS-0731503, and DMS-1016579, and by a UA Research Grants Committee Award.

The authors are with the Department of Mathematics, University of Alabama, Tuscaloosa, AL 35487 USA (e-mail: szhao@bama.ua.edu).

Color versions of one or more of the figures in this paper are available online at http://ieeexplore.ieee.org.

Digital Object Identifier 10.1109/TAP.2011.2161441

closure procedure is available for the MRTD methods to accommodate more complicated boundary conditions, such as the Robin/mixed condition. This greatly limits the possible application of the MRTD methods to more general electromagnetic calculations.

The objective of the present work is to construct a general procedure to implement nontrivial boundary conditions in the MRTD discretization. This is accomplished by introducing a fictitious domain boundary closure via the matched interface and boundary (MIB) method. For regular domain with straight boundaries, the MIB boundary scheme has been constructed for supporting arbitrarily high order central finite difference methods [16], [17]. Successive implementations of the MIB scheme for treating curved dielectric interfaces [22], [23] and curved PEC walls [24] have also been carried out. In the present study, to illustrate the proposed boundary closure scheme, the CDF S-MRTD method [12] will be employed. We note that the proposed procedure can be extended to other S-MRTD and W-MRTD methods. The rest of this paper is organized as the follows. Section II is devoted to the theory and algorithm of the MIB boundary closure scheme. Numerical tests involving Robin and time-dependent boundary conditions are carried out to validate the proposed method in Section III. Finally, a conclusion ends this paper.

II. Theory and Algorithm

A. Multiresolution Time-Domain (MRTD) Analysis

Assuming the absence of charge density and current source, and linear isotropic constitutive relations, we consider the transverse magnetic (TM) modes that are governed by the time-dependent two-dimensional (2D) Maxwell's equations

$$\epsilon\frac{\partial E_z}{\partial t}=\frac{\partial H_y}{\partial x}-\frac{\partial H_x}{\partial y} \tag{1}$$

$$\mu\frac{\partial H_x}{\partial t}=-\frac{\partial E_z}{\partial y},\quad \mu\frac{\partial H_y}{\partial t}=\frac{\partial E_z}{\partial x} \tag{2}$$

where E and H are, respectively, the normalized electric and magnetic field intensities and ϵ and μ are the relative electric permittitivy and magnetic permeability of material, respectively. Here, a nondimensional form of the equations is considered, i.e., $\epsilon=\mu=1$ in free space. Throughout, the medium is assumed to be nonmagnetic with $\mu=1$.

In the multiresolution time-domain (MRTD) analysis, basis functions can be chosen as scaling functions only or both scaling and wavelet functions. To illustrate the proposed boundary procedure, we concern ourselves with the S-MRTD schemes, i.e., using scaling functions only

$$E_z(x,y,t)=\sum_{i,j=-\infty}^{\infty}E^z_{i,j}(t)\phi_i(x)\phi_j(y) \tag{3}$$

$$H_x(x,y,t)=\sum_{i,j=-\infty}^{\infty}H^x_{i,j+\frac{1}{2}}(t)\phi_i(x)\phi_{j+\frac{1}{2}}(y) \tag{4}$$

$$H_y(x,y,t)=\sum_{i,j=-\infty}^{\infty}H^y_{i+\frac{1}{2},j}(t)\phi_{i+\frac{1}{2}}(x)\phi_j(y) \tag{5}$$

TABLE I
Coefficients for the CDF-MRTD Scheme [12]

	CDF(2,2)	CDF(2,4)	CDF(2,6)
$c(1)$	1.2291666667	1.2918129281	1.3110340773
$c(2)$	-0.0937500000	-0.1371343465	-0.1560100710
$c(3)$	0.0104166667	0.0287617723	0.0419957460
$c(4)$		-0.0034701413	-0.0086543236
$c(5)$		0.0000080265	0.0008308695
$c(6)$			0.0000108999
$c(7)$			-0.0000000041

where ϕ is an appropriate scaling function for the particular scheme being used, and the unknown field expansion coefficients $E^z_{i,j}(t)$, $H^x_{i,j+(1/2)}(t)$, and $H^y_{i+(1/2),j}(t)$ are time dependent. The staggered Yee grid can be naturally employed in such a MRTD expansion. In a homogeneous medium, the MRTD semi-discretization of Maxwell's equations (1) and (2) can be given as

$$\frac{\partial E^z_{i,j}(t)}{\partial t}=\sum_m\frac{c(m)}{\epsilon\Delta x}\left(H^y_{i+m-\frac{1}{2},j}(t)-H^y_{i-m+\frac{1}{2},j}(t)\right)-\sum_m\frac{c(m)}{\epsilon\Delta y}\left(H^x_{i,j+m-\frac{1}{2}}(t)-H^x_{i,j-m+\frac{1}{2}}(t)\right) \tag{6}$$

$$\frac{\partial H^x_{i,j+\frac{1}{2}}(t)}{\partial t}=-\sum_m\frac{c(m)}{\mu\Delta y}\left(E^z_{i,j+m}(t)-E^z_{i,j-m+1}(t)\right) \tag{7}$$

$$\frac{\partial H^y_{i+\frac{1}{2},j}(t)}{\partial t}=\sum_m\frac{c(m)}{\mu\Delta x}\left(E^z_{i+m,j}(t)-E^z_{i-m+1,j}(t)\right) \tag{8}$$

where Δx and Δy are the spacing in x and y directions. In the present MRTD calculations, the Cohen-Daubechies-Feauveau (CDF) MRTD coefficients [12] will be employed for $c(m)$ and are given in the Table I. For such MRTD methods, the spatial order of accuracy of the CDF(2,n) biorthogonal family is known to be $2+n$ [13]. Thus, the order of accuracy in space for the CDF(2,2), CDF(2,4), and CDF(2,6) MRTD schemes is, respectively, four, six, and eight. The temporal discretization of (6)–(8) can be simply formulated by using various standard time stepping methods. The classical fourth order Runge-Kutta method will be utilized such that both spatial and temporal orders of accuracy are at least four for the present MRTD analysis. However, the overall high order of accuracy of the present MRTD approach can still be impaired by deficient treatments of boundary conditions, particularly when complicated boundary conditions are encountered.

B. Image Principle

In the MRTD methods, the image principle is commonly used to deal with the perfect electric conducting (PEC) and perfect magnetic conducting (PMC) boundary conditions. This is a treatment to implement simple boundary conditions by assuming that there is a one-to-one correspondence between the inner grid node and the imaging fictitious node outside the domain. For example, for a problem with x interval being $x\in[a,b]$, consider a uniform grid $x_{-M}<\cdots<a=x_0<x_1<\cdots<x_N=b<\cdots<x_{N+M}$. Here the actual mesh size of the x partition is $N+1$, while M

represents the maximal number of fictitious points needed in a particular MRTD scheme, in order to ensure the MRTD spatial approximations (6)–(8) throughout the domain $[a, b]$. Consider the right boundary as an example and denote a function u to be either E or H. One could assume the following one-to-one image principle at the boundary

$$u(x_{N+j}) - u(x_N) = a_j \left[u(x_{N-j}) - u(x_N)\right] \tag{9}$$

for $j = 1, 2, \ldots, M$. In the PEC condition, we have $E_z = 0$ at the right end $x = b$. By using Maxwell's equations, one can further derive that $\partial^2 E_z/\partial x^2 = 0$ at $x = b$ [24]. Thus, the PEC condition for E_z can be satisfied by choosing $a_j = -1$ in (9). This is also called an anti-symmetric boundary extension [17]. The PEC condition for H_y, i.e., $\partial H_y/\partial x = 0$, can be imposed by taking $a_j = 1$ in (9). This is also called a symmetric boundary extension [17]. The image principle (9) can actually handle some boundary conditions that are more complicated than the PEC ones. Please see [17] for more details.

C. Matched Interface and Boundary (MIB) Treatment

However, for more general boundary conditions, such as the Robin condition, the image principle (9) can not be rigorously valid or can only be satisfied up to second order accuracy. Obviously, a more reasonable assumption is that a fictitious value $u(x_{N+j})$ should not depend on one inner value $u(x_{N-j})$ only, it should depend on *a set of* function values inside the boundary. This motivates the development of the matched interface and boundary (MIB) boundary scheme [16], [17].

We illustrate the idea by considering a Robin type boundary condition at $x = b$

$$\frac{\partial u}{\partial x} - ku = \phi(t). \tag{10}$$

The MIB boundary treatment assumes a function relation which is generalized from the image principle:

$$u(x_{N+j}) = \sum_{i=0}^{L} r_{i,j} u(x_{N-i}) + r_{L+1,j}\phi(t) \tag{11}$$

where $r_{i,j}$ are the MIB representation coefficients and $j = 1, 2, \ldots, M$. Thus, in the MIB discretization, each fictitious value outside the domain will depend on $L + 1$ inner values and one inhomogeneous boundary value $\phi(t)$. An iterative procedure is commonly used in the MIB method to determine these fictitious values one by one.

At the first step, since only one boundary condition is available, one can only determine one fictitious point $u(x_{N+1})$, see the Fig. 1. In the MIB scheme, the first derivative in the Robin condition (10) will be approximated by using one-sided finite difference with $L + 1$ grid points inside and one fictitious node outside. In particular, we choose $x = b$ as the differentiation point of the finite difference and denote it as the origin of the local grid stencil: $(-L\Delta x, \ldots, -\Delta x, 0, \Delta x)$. We denote the corresponding finite difference weights to be $(C_{-L}^{(L+2)}, \ldots, C_{-1}^{(L+2)}, C_0^{(L+2)}, C_1^{(L+2)})$. Here the subscript of the weight $C_i^{(L+2)}$ is for the local grid index, while the superscript represents the fact that there are totally $L + 2$ nodes in this stencil. Based on such a partition, the boundary condition (10) is discretized to be

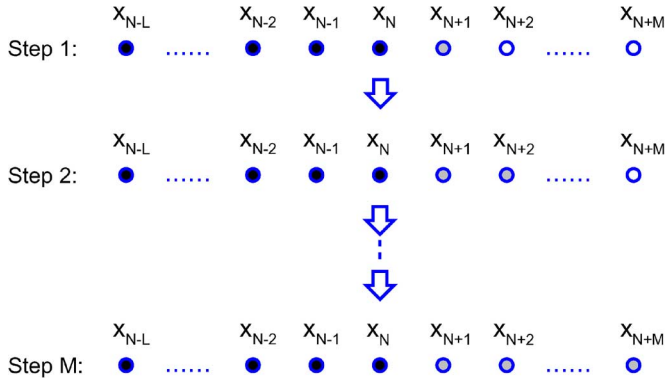

Fig. 1. Illustration of the MIB grid partition and the iterative procedure. Filled circles: regular nodes; Partially filled circles: solved fictitious nodes; Open circles: unsolved fictitious nodes.

$$\sum_{i=-L}^{1} C_i^{(L+2)} u(x_{N+i}) - ku(x_N) = \phi(t). \tag{12}$$

The only unknown $u(x_{N+1})$ in (12) can be solved in terms of other values, giving rise to the following representation coefficients: $r_{0,1} = (k - C_0^{(L+2)})/C_1^{(L+2)}$, $r_{L+1,1} = 1/C_1^{(L+2)}$, and $r_{i,1} = -C_{-i}^{(L+2)}/C_1^{(L+2)}$ for $i = 1, 2, \ldots, L$.

At the second step, we are about to determine the second fictitious value $u(x_{N+2})$, see Fig. 1. One possible way is to solve $u(x_{N+2})$ in a process similar to that in the first step, by also considering only one fictitious node outside the domain. A more accurate treatment is usually employed in the MIB scheme by considering two fictitious nodes simultaneously. The same boundary condition (10) is now discretized as

$$\sum_{i=-L}^{2} C_i^{(L+3)} u(x_{N+i}) - ku(x_N) = \phi(t) \tag{13}$$

where $C_i^{(L+3)}$ are the finite difference weights to approximate first derivative at $x = 0$ based on a local grid stencil: $(-L\Delta x, \ldots, -\Delta x, 0, \Delta x, 2\Delta x)$. Here the superscript indicates that there are totally $L + 3$ nodes involved in this approximation. From (13), one can solve $u(x_{N+2})$ in terms of the others. Then, the known representation coefficients for $u(x_{N+1})$ can be substituted in so that $u(x_{N+2})$ will also depend on $L + 1$ regular function values and $\phi(t)$. Consequently, the representation coefficients $r_{i,2}$ for $i = 0, \ldots, L + 1$ can be attained. Through such an iterative procedure, the total M fictitious points can be efficiently determined in M steps, see Fig. 1. The MIB treatment of other boundary conditions can be similarly carried out.

We note that in the MIB method, boundary conditions are enforced systematically so that it can achieve arbitrarily high orders in principle. In practice, the order of accuracy of the MIB scheme is dominated by the total number of interior support nodes L. One has certain flexibility in choosing L in the finite different approximation. A large L value is usually selected to ensure that the order of accuracy in the MIB boundary treatment is not less than that of the MRTD scheme. Nevertheless, for unsteady problems, a very large L may render the MIB method

unstable. The stability issue of the MIB method has been discussed in [17]. To guarantee the stability, one should choose L according to the upbounds established in [17].

An advantage of the generalized image principle (11) is that the representation coefficients $r_{i,j}$ are independent of the boundary data $\phi(t)$. Consequently, they are time invariant. Thus, the MIB scheme actually needs to be carried out only once at the beginning, even though $\phi(t)$ takes different value at different time. Therefore, the computational overhead introduced by the MIB boundary treatment is negligibly small in real MRTD computations. In summary, the MIB method provides a fictitious domain support so that the MRTD methods can be applied in a translation invariant manner throughout the domain. Furthermore, since the proposed MIB boundary treatment does not depend on the MRTD discretizations, this boundary closure scheme can be applied to other high order finite-difference time-domain (FDTD) methods.

III. Numerical Experiments

In this section, we examine the usefulness of the MIB boundary treatment by testing its robustness, accuracy, and convergence. Three MRTD schemes, i.e., the CDF(2,2), CDF(2,4), and CDF(2,6), are employed for the spatial discretization and the classical fourth order Runge-Kutta method is used for the temporal integration. Based on the given initial values at time $t = 0$, Maxwell's equations (1) and (2) will be solved until a stopping time $t = T$. Here we choose $T = 1$ for all tests in our non-dimensionalized unit system. A uniform grid is employed in all examples, with $N + 1$ being the mesh size along each direction. Unless otherwise specified, a small time increment $\Delta t = 10^{-4}$ is used to ensure that the temporal discretization error is negligible in our present tests. The absolute L_2 errors will be reported in all cases.

A. Example 1: Hollow Rectangular Waveguide

We first validate the MIB boundary closure scheme by considering a air filled rectangular waveguide with perfect conducting walls [9]. Designed to solve complicated boundary conditions, the MIB boundary closure scheme can also handle the simple PEC boundary conditions. Moreover, such a study actually enables us to compare the MIB boundary method with the image principle.

The cross section of the hollow waveguide is chosen as $(x, y) \in [0, a] \times [0, b]$. Such a simple structure permits analytical solutions:

$$\begin{aligned} E_z &= \sin\left(\frac{m\pi}{a}x\right)\sin\left(\frac{n\pi}{b}y\right)\cos(\omega t) \\ H_x &= -\frac{n\pi}{\mu\omega b}\sin\left(\frac{m\pi}{a}x\right)\cos\left(\frac{n\pi}{b}y\right)\sin(\omega t) \\ H_y &= \frac{m\pi}{\mu\omega a}\cos\left(\frac{m\pi}{a}x\right)\sin\left(\frac{n\pi}{b}y\right)\sin(\omega t) \end{aligned} \tag{14}$$

where $\omega = (1/\sqrt{\mu\epsilon})\sqrt{(m\pi/a)^2 + (n\pi/b)^2}$, and m and n are the wavenumbers. For the present example, two PEC conditions for magnetic components are involved: $\partial H_y/\partial x = 0$ at $x = 0$ and $x = a$, and $\partial H_x/\partial y = 0$ at $y = 0$ and $y = b$. For E_z, we originally have $E_z = 0$ at four PEC walls. According to Maxwell's equations, it is easy to derive two electric PEC conditions: $\partial^2 E_z/\partial x^2 = 0$ at $x = 0$ and $x = a$, and $\partial^2 E_z/\partial y^2 = 0$ at $y = 0$ and $y = b$. With little modification, the MIB treatment discussed in the previous section can be applied to solve these four PEC conditions.

TABLE II
The MRTD Results of Example 1 by Using the Image Principle

Scheme	Case 1	$N = 20$	$N = 40$	$N = 80$
CDF(2,2)	Error	$1.482(-3)$	$1.116(-4)$	$7.339(-6)$
	Order		3.73	3.93
CDF(2,4)	Error	$4.330(-4)$	$8.110(-6)$	$1.330(-7)$
	Order		5.74	5.93
CDF(2,6)	Error	$7.832(-5)$	$3.771(-7)$	$1.785(-9)$
	Order		7.70	7.72
	Case 2	$N = 20$	$N = 40$	$N = 80$
CDF(2,2)	Error	$2.641(-2)$	$3.689(-3)$	$2.737(-4)$
	Order		2.84	3.75
CDF(2,4)	Error	$3.461(-2)$	$1.075(-3)$	$1.989(-5)$
	Order		5.01	5.76
CDF(2,6)	Error	$2.180(-2)$	$1.944(-4)$	$9.248(-7)$
	Order		6.77	7.75

Here $1.482(-3)$ denotes 1.482×10^{-3}. In Case 1, $m = n = 5$ and in Case 2, $m = n = 10$.

TABLE III
The MRTD Results of Example 1 by Using the MIB Scheme

Scheme	Case 1	$N = 20$	$N = 40$	$N = 80$
CDF(2,2)	Error	$1.212(-3)$	$1.036(-4)$	$7.096(-6)$
	Order		3.55	3.87
CDF(2,4)	Error	$3.623(-4)$	$7.405(-6)$	$1.274(-7)$
	Order		5.61	5.86
CDF(2,6)	Error	$5.623(-5)$	$3.012(-7)$	$1.968(-9)$
	Order		7.54	7.26
	Case 2	$N = 20$	$N = 40$	$N = 80$
CDF(2,2)	Error	$2.092(-2)$	$3.363(-3)$	$2.638(-4)$
	Order		2.64	3.67
CDF(2,4)	Error	$2.761(-2)$	$9.860(-4)$	$1.903(-5)$
	Order		4.81	5.70
CDF(2,6)	Error	$2.418(-2)$	$1.663(-4)$	$8.326(-7)$
	Order		7.18	7.64

In Case 1, $m = n = 5$ and in Case 2, $m = n = 10$.

In the present computations, the initial values are taken according to the analytical solutions. The physical parameters are chosen as $a = b = 1$ and $\epsilon = \mu = 1$. Two test cases are examined with $m = n = 5$ in Case 1 and $m = n = 10$ in Case 2. The high frequency solutions in Case 2 are particularly important to investigate the performance of high order methods. The numerical results of the image principle and the MIB boundary scheme are listed, respectively, in Table II and Table III.

The image principle is obviously satisfied for the present analytical solutions (14). Thus, the numerical errors reported in Table II are primarily due to the MRTD spatial discretizations. As mentioned above, the order of accuracy for the CDF(2,2), CDF(2,4), and CDF(2,6) MRTD schemes is, respectively, four, six, and eight. Such orders have been numerically verified in the low frequency case and the high frequency case with a large N.

With the confidence of the present MRTD spatial discretization, we now turn to the MIB boundary closure. A large enough L is used in the MIB scheme. In particular, we choose $L = 3$, 5, and 7, respectively, for the CDF(2,2), CDF(2,4), and CDF(2,6) MRTD schemes. It can seen from the Table III that the MIB results are in good agreement with those of the image principle,

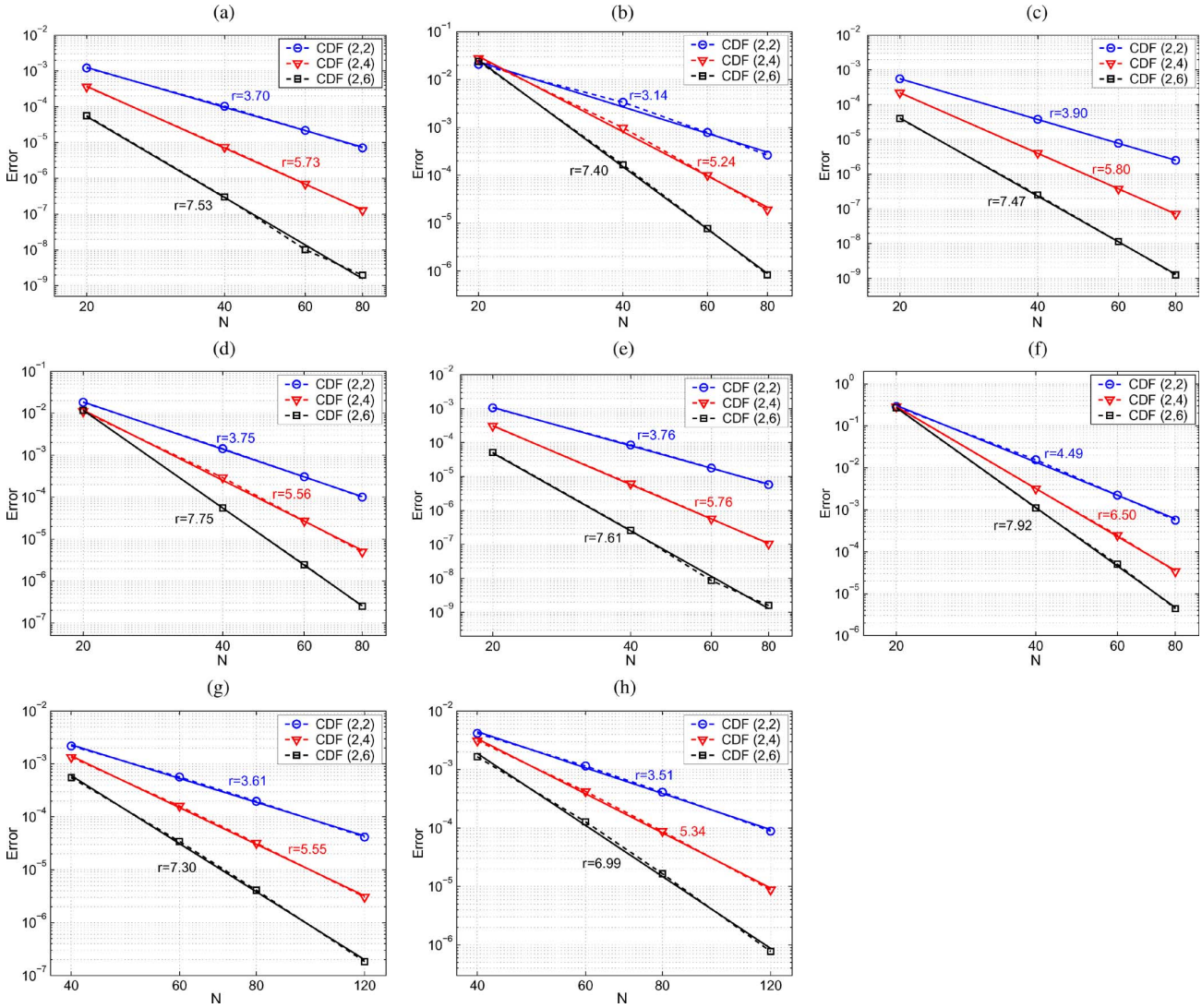

Fig. 2. Numerical convergence rates of the MIB-MRTD method. (a) Example 1, Case 1; (b) Example 1, Case 2; (c) Example 2, Case 1; (d) Example 2, Case 2; (e) Example 3, Case 1; (f) Example 3, Case 2; (g) Example 4, Case 1; (h) Example 4, Case 2. In all cases, the solid line represents the least squares fitted linear trend. The slope of this line reveals the overall numerical order of the spatial discretization, and is labeled on the graph.

with very minor differences. This validates the MIB boundary closure scheme.

We further examine the order of convergence of the MIB-MRTD spatial discretization by plotting the numerical errors in chart (a) and (b) of Fig. 2. These errors are shown as dashed lines. A linear fitting by means of the least squares is then conducted for each case in the log-log scale. The corresponding fitted convergence lines are depicted as solid lines in Fig. 2. Moreover, the fitted slope essentially represents the numerical convergence rate r of the MIB-MRTD method. These rates are shown in Fig. 2 too. It is interesting to note that there are some differences between the convergence patterns of the low frequency test (Case 1) and the high frequency test (Case 2). It is known that the high frequency test is challenging to low order methods or coarse numerical meshes. Thus, the overall rate of CDF(2,2) for the Case 2 is only $r = 3.14$, although it attains a value of 3.67 when $N = 80$ in Table III. On the other hand, with $N = 20$, all three MRTD schemes perform poorly. We even have that the higher order method yields a larger error. This is because the grid resolution is too low in this case, i.e., only 4 grid points per wavelength (PPW). With such a low PPW, only spectral type methods, such as pseudospectral time-domain (PSTD) methods [4], [5] or local spectral time-domain (LSTD) methods [8], [9], can deliver reasonable accuracy. For the present problem, the MRTD methods perform better when N is larger. Eventually, the numerical orders of both the CDF(2,4) the CDF(2,6) are quite close to the theoretical ones.

The currently chosen MIB parameter values of L are within the upbounds given in [17] so that the MIB-MRTD computations are guaranteed to be conditionally stable. An interesting question next is whether the MIB scheme will affect the Courant-Friedrichs-Levy (CFL) factor of the underlying MRTD method or not. To this end, we detect the numerical CFL numbers of the MRTD discretization with or without MIB boundary closure. In particular, we consider the Case I with $N = 40$ and a stopping time $T = 20$. Denote the total number of time steps to be N_t. We have $N_t = T/\Delta t$. We numerically

TABLE IV
THE NUMERICAL CFL NUMBERS FOR EXAMPLE 1

Scheme	MRTD		MIB-MRTD		
	N_t	CFL	L	N_t	CFL
CDF(2,2)	1060	0.7547	3	1061	0.7540
CDF(2,4)	1162	0.6885	5	1162	0.6885
CDF(2,6)	1207	0.6628	7	1206	0.6633

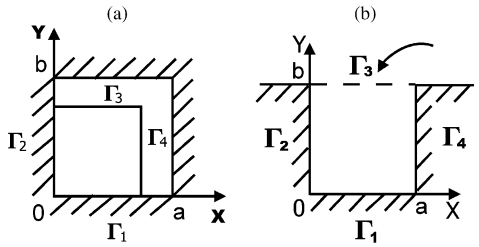

Fig. 3. Computational domain of Example 2 (left) and Example 3 (right).

search for the critical N_t values such that the computation is still stable. Then, the numerical CFL number is reported to be $T/(\Delta x N_t)$. See Table IV. It is clear that the CFL numbers with and without MIB scheme are essentially the same. This is in consistent with our previous findings that for hyperbolic equations, the MIB method maintains the same CFL number as the underlying spatial method whenever it is stable [17].

B. Example 2: Shifted Computational Domain

We next study a synthetic example based on the hollow rectangular waveguide. Consider the same physical setting as in the Example 1, but with a shifted computational domain $(x, y) \in [0, (3/4)a] \times [0, (4/5)b]$. Denote four boundaries of this new domain to be Γ_1, Γ_2, Γ_3, and Γ_4, see Fig. 3(a). We then have that the PEC conditions are not valid on Γ_3 and Γ_4, although the same analytical solutions are assumed. Instead, the correct boundary conditions are constructed as the follows:

$$\frac{\partial^2 E_z}{\partial x^2} + \left(\frac{m\pi}{a}\right)^2 E_z = 0, \quad \text{on} \quad \Gamma_4 \tag{15}$$

$$\frac{\partial^2 E_z}{\partial y^2} + \left(\frac{n\pi}{b}\right)^2 E_z = 0, \quad \text{on} \quad \Gamma_3 \tag{16}$$

$$\frac{\partial^2 H_y}{\partial x^2} + \left(\frac{m\pi}{a}\right)^2 H_y = 0, \quad \text{on} \quad \Gamma_4 \tag{17}$$

$$\frac{\partial^2 H_x}{\partial y^2} + \left(\frac{n\pi}{a}\right)^2 H_x = 0, \quad \text{on} \quad \Gamma_3. \tag{18}$$

The image principle obviously cannot handle these complicated boundary conditions.

The MIB treatment of two E_z conditions (15) and (16) can be carried out similarly. Nevertheless, a subtle point needs to be taken care of in solving magnetic boundary conditions (17) and (18). We illustrate this by considering (17) as an example. By using a staggered grid, there is actually no grid node for H_y located exactly on the boundary point $x = (3/4)a$. Thus, the second term in (17), i.e., $(m\pi/a)^2 H_y$, cannot be directly evaluated in the MIB discretization. Instead, the H_y value shall be interpolated based on the same grid stencil used for approximating the second derivative. In this manner, the MIB scheme can be proceeded as in the previous studies.

TABLE V
THE RESULTS OF THE MIB-MRTD METHOD FOR EXAMPLE 2

Scheme	Case 1	$N = 20$	$N = 40$	$N = 80$
CDF(2,2)	Error	$5.544(-4)$	$3.770(-5)$	$2.486(-6)$
	Order		3.88	3.92
CDF(2,4)	Error	$2.186(-4)$	$4.036(-6)$	$7.078(-8)$
	Order		5.76	5.83
CDF(2,6)	Error	$3.977(-5)$	$2.502(-7)$	$1.251(-9)$
	Order		7.31	7.64
	Case 2	$N = 20$	$N = 40$	$N = 80$
CDF(2,2)	Error	$1.825(-2)$	$1.431(-3)$	$1.003(-4)$
	Order		3.68	3.83
CDF(2,4)	Error	$1.101(-2)$	$2.920(-4)$	$4.951(-6)$
	Order		5.24	5.88
CDF(2,6)	Error	$1.179(-2)$	$5.506(-5)$	$2.513(-7)$
	Order		7.74	7.78

In Case 1, $m = n = 5$ and in Case 2, $m = n = 10$.

The numerical results of the MIB-MRTD method are reported in Table V. These results are also depicted in chart (c) and (d) of Fig. 2. It can be seen that the MIB-MRTD schemes attain the correct numerical orders in both low and high frequency tests. Furthermore, the convergence patterns of the high frequency case become better, in comparing with those of the Example 1. This is because a smaller computation domain in the Example 2 actually implies a larger PPW. The present result shows that the overall performance of the MIB scheme in handling complicated boundaries is satisfactory.

C. Example 3: Rectangular Open Cavity

We then consider a 2D rectangular open cavity embedded in an infinite ground plane, see Fig. 3(b). The study of electromagnetic scattering by such a cavity is of great industrial and military interests, because the open cavity can be regarded as a prototype structure of a more realistic one, such as a jet engine inlet duct or exhaust nozzle [25]. Denote the width of the cavity as a and the depth as b. The cavity walls and ground plane are usually assumed to be PEC boundaries. The original cavity problem is defined on cavity and the half space above the ground plane with Sommerfeld's radiation conditions imposed at infinity. A modern approach to solve cavity problem is to introduce a transparent boundary condition above the cavity [25], i.e., along Γ_3 in Fig. 3(b). This induces a computational domain $(x, y) \in [0, a] \times [0, b]$ within the rectangular cavity.

In the present study, we numerically solve 2D Maxwell's equations (1) and (2) within the rectangular cavity. To benchmark our numerical results, a set of analytical solutions is constructed as the follows:

$$\begin{aligned} E_z &= \sin\left(\frac{n\pi}{a}x\right)\sinh(ky)\cos(\omega t) \\ H_x &= -\frac{k}{\mu\omega}\sin\left(\frac{n\pi}{a}x\right)\cosh(ky)\sin(\omega t) \\ H_y &= \frac{n\pi}{\mu\omega a}\cos\left(\frac{n\pi}{a}x\right)\sinh(ky)\sin(\omega t) \end{aligned} \tag{19}$$

where $\omega = (1/\sqrt{\mu\epsilon})\sqrt{(n\pi/a)^2 - k^2}$, and n and k are the wavenumbers. Note that the time harmonic part of the analytical solution (19) actually represents a single mode of the mode-

TABLE VI
THE RESULTS OF THE MIB-MRTD METHOD FOR EXAMPLE 3

Scheme	Case 1	$N=20$	$N=40$	$N=80$
CDF(2,2)	Error	$1.059(-3)$	$8.537(-5)$	$5.764(-6)$
	Order		3.63	3.89
CDF(2,4)	Error	$3.081(-4)$	$6.109(-6)$	$1.035(-7)$
	Order		5.66	5.88
CDF(2,6)	Error	$5.151(-5)$	$2.602(-7)$	$1.594(-9)$
	Order		7.63	7.35
	Case 2	$N=20$	$N=40$	$N=80$
CDF(2,2)	Error	$2.885(-1)$	$1.552(-2)$	$5.663(-4)$
	Order		4.22	4.78
CDF(2,4)	Error	$2.874(-1)$	$3.183(-3)$	$3.400(-5)$
	Order		6.50	6.55
CDF(2,6)	Error	$2.719(-1)$	$1.104(-3)$	$4.395(-6)$
	Order		7.94	7.97

In Case 1, $n=5$ and $k=1$ and in Case 2, $n=10$ and $k=5$.

matching solution which converges to the exact solution of the scattering problem [25]. With the PEC conditions on Γ_1, Γ_2, and Γ_4, the Robin type boundary conditions are assumed on Γ_3:

$$\frac{\partial E_z}{\partial y} - kE_z = k\sin\left(\frac{n\pi x}{a}\right)\cos(\omega t)e^{-kb} \tag{20}$$

$$\frac{\partial H_x}{\partial y} - kH_x = \frac{k^2}{\mu\omega}\sin\left(\frac{n\pi x}{a}\right)\sin(\omega t)e^{-kb}. \tag{21}$$

The MIB scheme for conditions (20) and (21) can be carried out exactly as what was described in Section II. We note that even though the boundary data ϕ is a spatial function along the boundary and time variant, i.e., $\phi(x,t)$, the MIB representation coefficients solved from boundary conditions (20) and (21) are still time independent and x independent. Thus, it is sufficient to conduct the MIB treatment only once. The solved representation coefficients can then be applied at any time t and at any x node along Γ_3. Therefore, the MIB boundary treatment is computationally very efficient.

In the present study, the physical parameters are chosen as $a=b=1$ and $\epsilon=\mu=1$. Again, two test cases are studied with $n=5$ and $k=1$ in Case 1 and $n=10$ and $k=5$ in Case 2. The numerical results are shown in Table VI and chart (e) and (f) of Fig. 2. It can be seen that the correct spatial order of accuracy is achieved in all tests. We note that the MRTD errors are greater than 0.2 when $N=20$ for the high frequency case. This is because the present solution is highly oscillatory along x direction, while is subject to a very rapid exponential growth along y direction. See Fig. 4. Such a solution is very difficult to be resolved on a coarse grid. Nevertheless, when we refine the mesh, a satisfactory accuracy is achieved by the MIB-MRTD scheme.

D. Example 4: A Test Without Analytical Solution

We finally consider a test without analytical solution. The hollow rectangular waveguide with four PEC boundaries in the Example 1 is studied again. However, we consider the structure being excited by Gaussian type pulses initially. Such a study can be used to numerically predict the cutoff frequencies of the structure [9]. Two initial values of E_z are considered

$$E_z(x,y,0) = Ae^{-\frac{\left(x-\frac{a}{2}\right)^2+\left(y-\frac{b}{2}\right)^2}{2\sigma^2}} \tag{22}$$

$$E_z(x,y,0) = Ae^{-\frac{\left(x-\frac{a}{2}\right)^2+\left(y-\frac{b}{2}\right)^2}{2\sigma^2}}\sin\left(\frac{5\pi}{a}x\right)\sin\left(\frac{5\pi}{b}x\right) \tag{23}$$

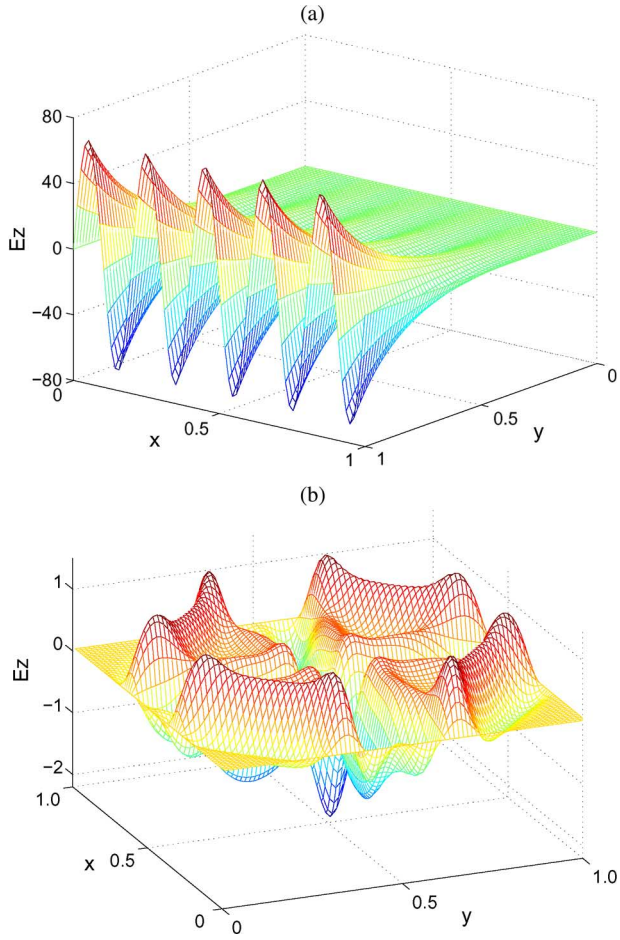

Fig. 4. Plot of numerical solution E_z at time $t=1$ by using the CDF(2,6) and $N=80$. (a): Example 3, Case 2; (b): Example 4, Case 2.

respectively, for Case 1 and Case 2, while the initial values of H_x and H_y are chosen as zero. Here $a=b=1$, $A=10$, and $\sigma=0.05$. The PEC conditions hold in Case 2, while the initial solution of Case 1 satisfies the PEC conditions approximately, since the Gaussian decays to a negligibly small values at the boundaries. We then integrate Maxwell's equations to $T=1$. No analytical solution is available to benchmark our MIB results. Thus, an "exact solution" obtained by the MIB-MRTD with CDF(2,6) and a dense mesh $N=240$ is used as the reference. In comparing with the reference solution, the MIB-MRTD errors are shown in Table VII and chart (g) and (h) of Fig. 2. It can be seen that the correct orders are numerically achieved, even though the solution is highly irregular, see Fig. 4(b).

IV. CONCLUSION

In conclusion, we have introduced a novel boundary closure scheme, the matched interface and boundary (MIB) method, for the treatment of general boundary conditions in the multiresolution time-domain (MRTD) calculations of Maxwell's equations. In the MIB method, boundary conditions are repeatedly utilized to systematically determine a set of fictitious values outside the domain. Consequently, the MRTD approximation can be applied in a translation invariant manner near the boundary.

TABLE VII
THE RESULTS OF THE MIB-MRTD METHOD FOR EXAMPLE 4

Scheme	Case 1	$N = 30$	$N = 60$	$N = 120$
CDF(2,2)	Error	$4.633(-3)$	$5.669(-4)$	$4.155(-5)$
	Order		3.03	3.77
CDF(2,4)	Error	$4.928(-3)$	$1.602(-4)$	$3.036(-6)$
	Order		4.94	5.72
CDF(2,6)	Error	$3.056(-3)$	$3.435(-5)$	$1.832(-7)$
	Order		6.48	7.55
	Case 2	$N = 30$	$N = 60$	$N = 120$
CDF(2,2)	Error	$8.255(-3)$	$1.154(-3)$	$8.840(-5)$
	Order		2.84	3.71
CDF(2,4)	Error	$1.005(-2)$	$4.218(-4)$	$8.731(-6)$
	Order		4.57	5.59
CDF(2,6)	Error	$7.225(-3)$	$1.277(-4)$	$7.744(-7)$
	Order		5.82	7.37

Several numerical experiments have been carried out to demonstrate the robustness of the MIB scheme in handling complicated boundary conditions, such as Robin and/or time-dependent ones. The MIB boundary treatment can achieve arbitrarily high order accuracy in principle. In the present study, the MIB orders are guaranteed to be not less than that of the underlying MRTD spatial discretization, so that the MIB-MRTD methods achieve the theoretical orders in all numerical tests. The MIB coefficient generation can be carried out only once to deal with boundary conditions with spatial and temporal dependent inhomogeneous terms. Thus, the MIB boundary treatment is computationally cheap. The MIB fictitious domain treatment does not assume any *a priori* knowledge of wave solutions, so that it has no limitation to be applied to real world electromagnetic problems. The MIB treatment of nontrivial boundary conditions on irregular domains is currently under our consideration.

REFERENCES

[1] J. Fang, "Time domain finite difference computation for Maxwell's equations," Ph.D. dissertation, Department of Electrical Engineering, Univ. California, Berkeley, CA, 1989.

[2] M. Krumpholz and L. P. B. Katehi, "New time-domain schemes based on multiresolution analysis," *IEEE Trans. Microw. Theory Tech.*, vol. 44, pp. 555–571, 1996.

[3] L. P. B. Katehi, J. F. Harvey, and E. Tentzeris, "Time-domain analysis using multiresolution expansions," in *Advances in Computational Electrodynamics: The Finite-Difference Time-Domain Method*, A. Taflove, Ed. Boston, MA: Artech House, 1998.

[4] Q. H. Liu, "The PSTD algorithm: A time-domain method requiring only two cells per wavelength," *Microw. Opt. Techn. Lett.*, vol. 15, pp. 158–165, 1997.

[5] Q. H. Liu, "Large-scale simulations of electromagnetic and acoustic measurements using the pseudospectral time-domain (PSTD) algorithm," *IEEE Trans. Geosci. Remote Sens.*, vol. 37, pp. 917–926, 1999.

[6] S. Wang, F. L. Teixeira, R. Lee, and J.-F. Lee, "Dispersion-relation preserving (DRP) 2D finite-difference time-domain schemes," in *Proc. IEEE Antennas Propag. Soc. Int. Symp.*, San Antonio, Tx, 2002, vol. 3, pp. 264–267.

[7] S. Wang and F. L. Teixeira, "Dispersion-relation-preserving (DRP) FDTD algorithms for large-scale three dimensional problems," *IEEE Trans. Antennas Propag.*, vol. 51, pp. 1818–1828, 2003.

[8] G. Bao, G. W. Wei, and S. Zhao, "Local spectral time-domain method for electromagnetic wave propagation," *Opt. Lett.*, vol. 28, pp. 513–515, 2003.

[9] Z. H. Shao, G. W. Wei, and S. Zhao, "DSC time-domain solution of Maxwell's equations," *J. Comput. Phys.*, vol. 189, pp. 427–453, 2003.

[10] X. Wei, E. Li, and C. Liang, "A new MRTD scheme based on Coifman scaling functions for the solution of scattering problems," *IEEE Microw. Wireless Compon. Lett.*, vol. 12, pp. 392–394, 2002.

[11] M. Fujii and W. J. R. Hoefer, "Time-domain wavelet Galerkin modeling of two-dimensional electrically large dielectric waveguides," *IEEE Trans. Microw. Theory Tech.*, vol. 49, pp. 886–892, 2001.

[12] T. Dogaru and L. Carin, "Multiresolution time-domain using CDF biorthogonal wavelets," *IEEE Trans. Microw. Theory Tech.*, vol. 49, pp. 902–912, 2001.

[13] N. Kovvali, W. Lin, and L. Carin, "Order of accuracy analysis for multiresolution time-domain using Daubechies bases," *Microw. Opt. Tech. Lett.*, vol. 45, pp. 290–293, 2005.

[14] Q. S. Cao, R. Kanapady, and F. Reitich, "High-order Runge-Kutta multiresolution time-domain methods for computational electromagnetics," *IEEE Trans. Microw. Theory Tech.*, vol. 54, pp. 3316–3326, 2006.

[15] K. L. Shlager and J. B. Schneider, "Comparison of the dispersion properties of higher order FDTD schemes and equivalent-sized MRTD schemes," *IEEE Trans. Antennas Propag.*, vol. 52, pp. 1095–1104, 2004.

[16] S. Zhao, "On the spurious solutions in the high-order finite difference methods," *Comput. Method Appl. Mech. Engrg.*, vol. 196, pp. 5031–5046, 2007.

[17] S. Zhao and G. W. Wei, "Matched interface and boundary (MIB) method for the implementation of boundary conditions in high-order central finite differences," *Int. J. Numer. Method Engrg.*, vol. 77, pp. 1690–1730, 2009.

[18] E. M. Tentzeris, R. L. Robertson, J. F. Harvey, and L. P. B. Katehi, "PML absorbing boundary conditions for the characterization of open microwave circuit components using multiresolution time-domain techniques (MRTD)," *IEEE Trans. Antennas Propag.*, vol. 47, pp. 1709–1715, 1999.

[19] Q. S. Cao, Y. C. Chen, and R. Mittra, "Multiple image technique (MIT) and anisotropic perfectly matched layer (APML) in implementation of MRTD scheme for boundary truncations of microwave structures," *IEEE Trans. Microw. Theory Tech.*, vol. 50, pp. 1578–1589, 2002.

[20] M. Peschke and W. Menzel, "Investigation of boundary algorithm for multiresolution analysis," *IEEE Trans. Microw. Theory Tech.*, vol. 51, pp. 1262–1268, 2003.

[21] N. Kovvali, W. Lin, and L. Carin, "Image technique for multiresolution time-domain using nonsymmetric basis functions," *Microw. Opt. Tech. Lett.*, vol. 47, pp. 44–47, 2005.

[22] S. Zhao, "High order vectorial analysis of waveguides with curved dielectric interfaces," *IEEE Microw. Wireless Compon. Lett.*, vol. 19, pp. 266–268, 2009.

[23] S. Zhao, "High order matched interface and boundary methods for the Helmholtz equation in media with arbitrarily curved interfaces," *J. Comput. Phys.*, vol. 229, pp. 3155–3170, 2010.

[24] S. Zhao, "A fourth order finite difference method for waveguides with curved perfectly conducting boundaries," *Comput. Method Appl. Mech. Engrg.*, vol. 199, pp. 2655–2662, 2010.

[25] G. Bao and W. Zhang, "An improved mode-matching method for large cavities," *IEEE Antennas Wireless Propag. Lett.*, vol. 4, pp. 393–396, 2005.

Pengfei Yao was born in Hangzhou, China, in 1983. He received the B.Sc degree in mathematics from Shantou University, China, in 2006.

Currently, he is a graduate student in the Department of Mathematics, The University of Alabama, Tuscaloosa. His research interests include high order numerical methods for partial differential equations, and computational electromagnetics.

Shan Zhao was born in Guiyang, China, in 1974. He received the B.Sc. degree in mathematics from Lanzhou University, China, in 1997 and the Ph.D. degree in scientific computing from the National University of Singapore, in 2003.

From 2003 to 2006, he was a Postdoctoral Fellow with Michigan State University. In 2006, he joined the faculty of the Mathematics Department, University of Alabama, Tuscaloosa, as an Assistant Professor. His current research interests include high order methods for partial differential equations, fast electromagnetic simulation in inhomogeneous media, and mathematical modeling of biomolecular surfaces.